MAGNETOSONIC WAVES AND THEIR RELATIONSHIPS WITH ENERGETIC PROTONS

S. Perraut, P. Robert and A. Roux⁽¹⁾, A. Korth, G. Kremser⁽²⁾, J. A. Sauvaud and J. M. Bosqued⁽³⁾

ABSTRACT

Monochromatic waves with frequencies close to/or above the proton gyroharmonics have frequently been observed in the vicinity of the geomagnetic equator by the GEOS spacecraft. These waves generally consist of harmonically-related emissions and propagate in a direction perpendicular to the DC magnetic field. The frequency spectrum is indicative of a strong nonlinear coupling between the various components of the spectrum.

Two different energy sources have been identified for destabilizing these waves: a ring-like distribution of ~10 keV protons and a sharp drift boundary of these protons. Both kinds of proton distributions can excite a non resonant instability (flute mode) near the proton gyrofrequency and its harmonics. Experimental results will be discussed and compared to growth rate calculations.

Keywords: Ring Current Proton Instability, Magnetosonic Waves Generation

1. INTRODUCTION

In addition to Ion Cyclotron Waves (ICW's) that are commonly observed at the geostationary orbit (Roux et al., this issue), Magnetosonic Waves (MSW's hereafter) have been detected only recently on board the European GEOS 1 and 2 satellites, owing to the high sensitivity of the search-coils which equipped these spacecraft (Refs. 1 and 2). The existence of these waves was reported earlier in Ref. 3 with data from the OGO 3 spacecraft and in Ref. 4 with data from IMP 6 and Hawkeye 1.

From the continuous observations of ULF waves between 0.2 and 11.5 Hz, the principal characteristics of these MSW's have been established: this is discussed in

- (1) Centre de Recherches en Physique de l'Environnement, CNET, 38-40 rue du Général Leclerc, 92131 Issy-les-Moulineaux, France
- Max-Planck-Institut für Aeronomie, 3411 Katlenburg-Lindau 3, FRG.
- (3) Centre d'Etude Spatiale des Rayonnements, B.P. 4346, 31029 Toulouse-Cédex, France

Section 2. In the third Section, it is shown that MSW's can be destabilized by a ring like distribution of ions having energies ~10 keV (Ref. 2). Section 4 will be devoted to the relationship between MSW's and sharp pressure gradients in the ion distribution, which are observed in the noon sector (Ref. 5).

2. PRINCIPAL CHARACTERISTICS

2.1 Polarization

On Figure 1 (August 23, 1978) the three components of MSW emission recorded between 0.2 and 10 Hz are plotted. The Bz component which is almost aligned with the DC magnetic field B is more intense than the B_L and B_R components which correspond to the left and right-hand polarized components in a plane perpendicular to B respectively.

2.2 Harmonic structure

The harmonic structure of MSW's is a general feature which can also be clearly identified in Figure 1. The emission starts at 15.37 UT exactly at the proton gyrofrequency. From thereon it splits up into three independent emissions. The first has a frequency which decreases with time; let us call it the emission at f_1 . The two others have frequencies that increase with time, f_2 and f_3 . While f_1 is below F_{H^+} , f_2 and f_3 are above it; therefore the harmonic structure does not depend upon the frequency of the fundamental. This harmonic structure is not due to nonlinear effects occurring in the detecting system.

2.3 Frequency range

MSW's generally have their fundamental around or above F_{H^+} . Occasionally, theses emissions can be detected well below F_{H^+} , with a fundamental between F_{He^+} and $2F_{He^+}$, in a frequency range where ICW's are often observed. In particular, just after a strong compression of the magnetosphere, emissions with a polarization parallel to \overline{B}_{O} have been observed around F_{He^+} (Figure 2); thus MSW's should be characterized by their polarization rather than by their frequency range. Moreover the frequency range covered by these emissions can exceed the Nyquist frequency (11.5 Hz) of the ULF experiment.

2.4 Nonlinear coupling

For intense MSW's, the harmonic structure may be the consequence of wave-wave coupling. Figure 1 is an illustration of this; around 16.30 UT, a detailed spectrum

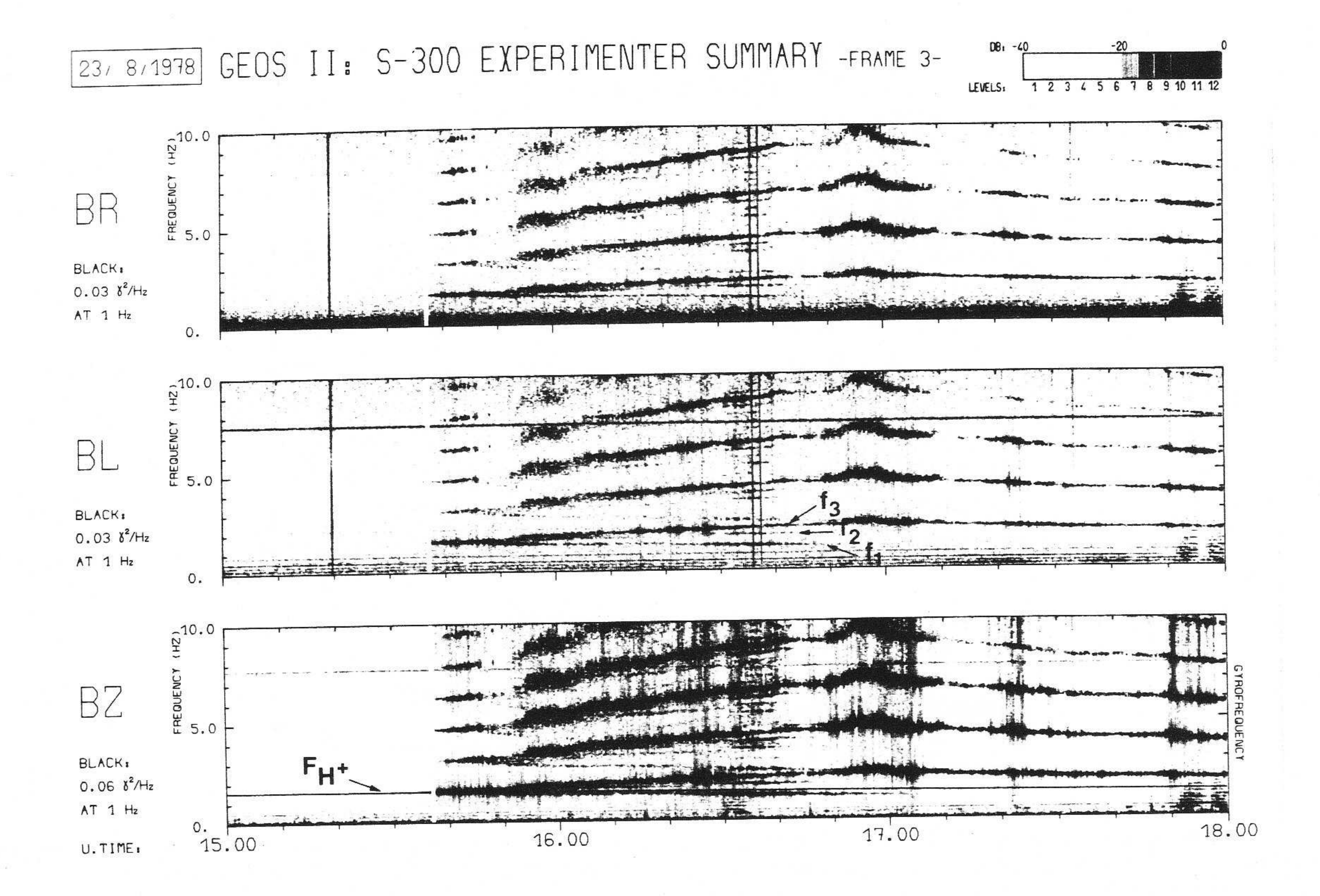


Figure 1. Frequency-time spectrograms of ULF waves observed on August 23, 1978, on GEOS 2. The three panels refer to right handed (B_R), left-handed (B_L) and parallel to the spin axis (B_Z) components. The angle between the spin axis and the dc magnetic field θ is ~13°, the distance 6,6 R_F , and the magnetic latitude $\lambda_m = -3$ °; LT = UT + 2 hours, 18 mn. The cold plasma density $N_0 \simeq 45$ cm 3 . Three different fundamentals f_1 , f_2 and f_3 can be seen.

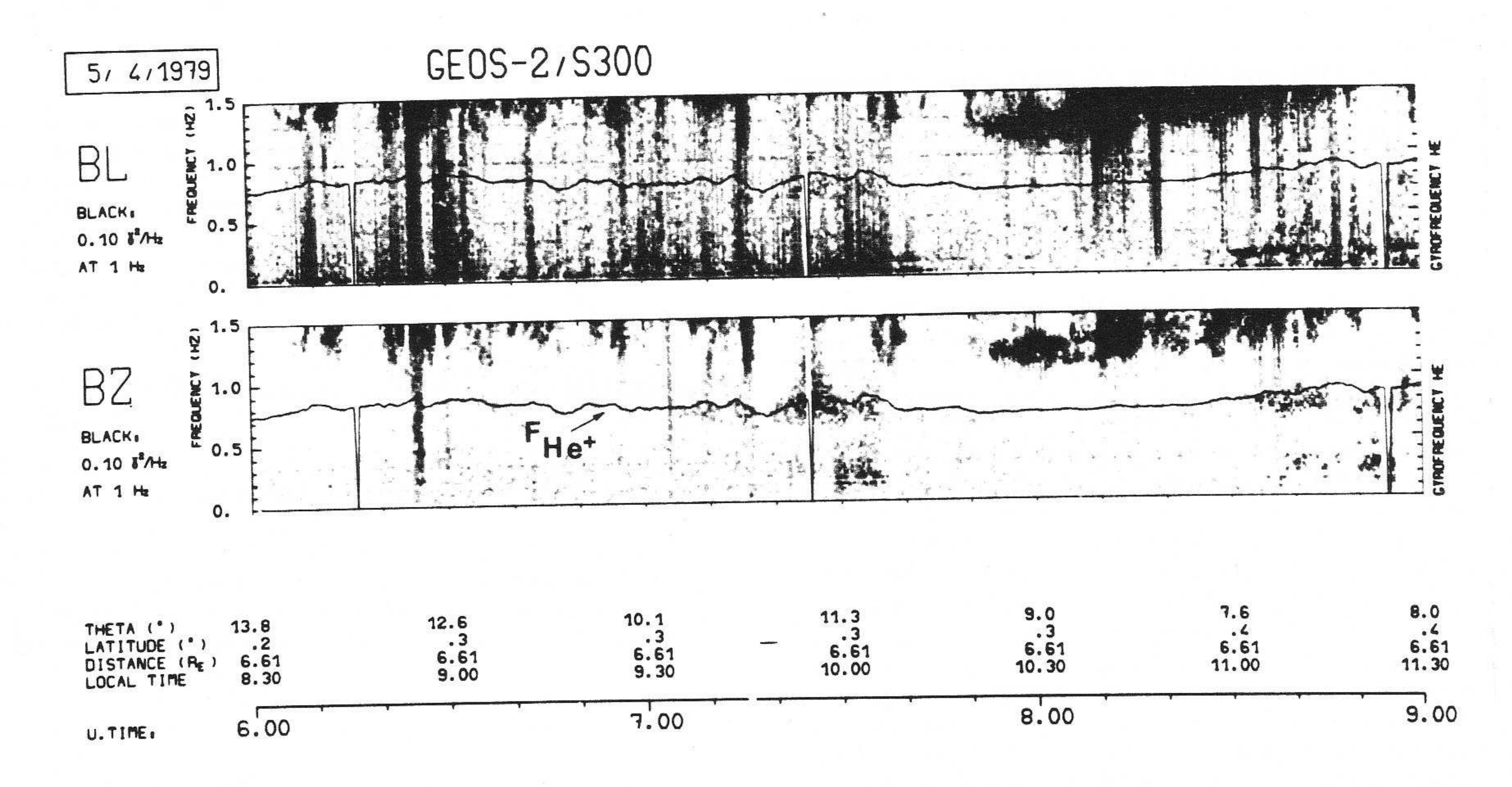


Figure 2. Frequency-time spectrograms MSW's observed on April 5, 1979, on GEOS 2. The frequency range is 0 to 1.5 Hz. Around 07.30 and 08.30 UT, emissions just below F_{He}^+ are observed predominently on the B_Z component.

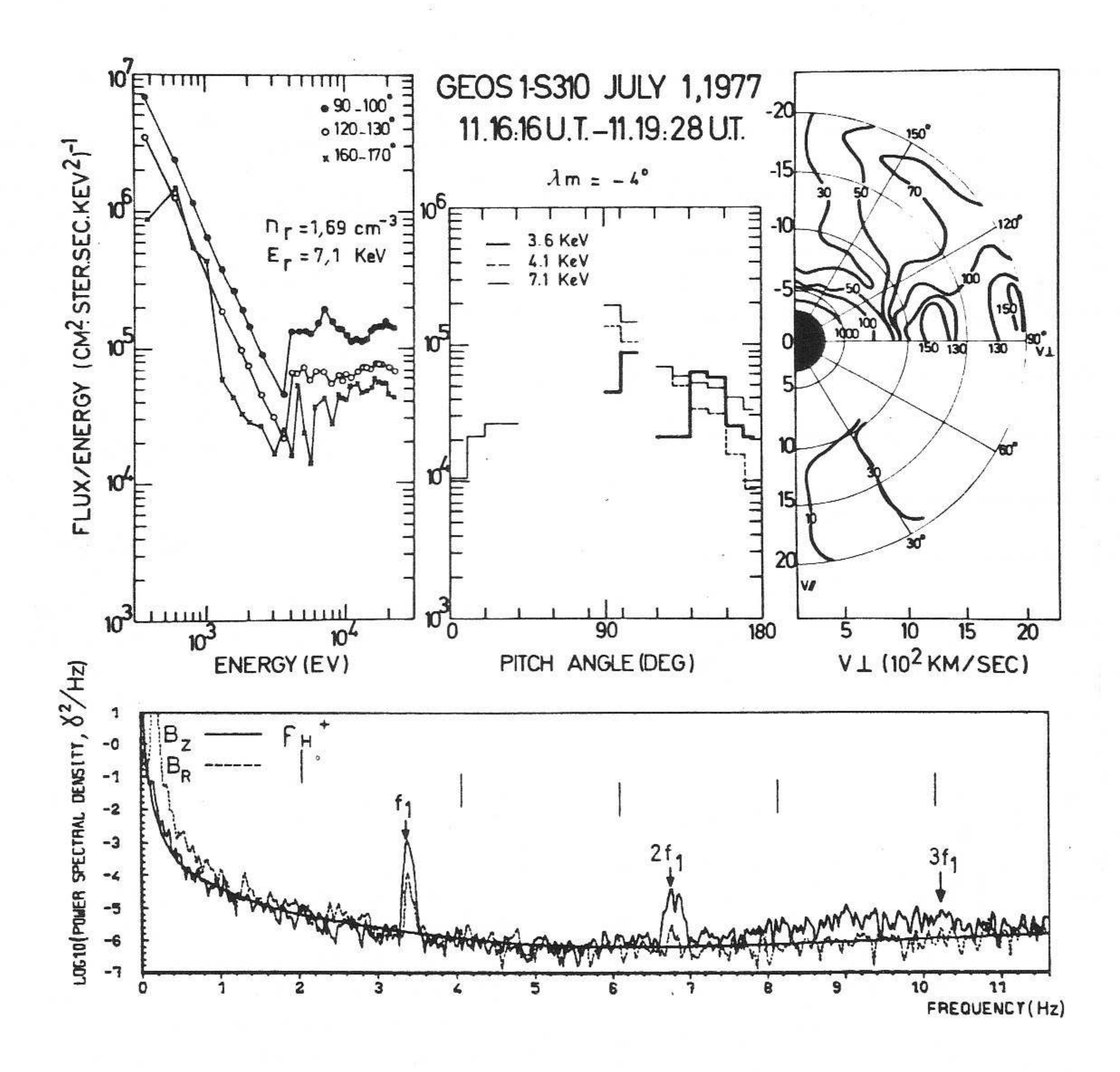


Figure 3. Comparison between MSW's and energetic protons July 1, 1977 at L=6.25. The energy, pitch angle distributions, and distribution functions f(V) in the velocity space measured over ~ 3 min are drawn on the top. Two-dimensional isocontours of $f(V_1, V_1)$ are labelled in units of 10^3 (cm²s sr keV²) . A peak at 7 keV and on the 90° pitch angle is clearly seen (two left panels). Two different maxima in the direction perpendicular to B_0 are evidenced (right panel). $\partial f/\partial V_1$ is >0 in the close vicinity of these peaks. The wave power spectrum computed simultaneously is drawn below. A change of reference frame was performed to align B_2 with respect to B_0 . F_1 , and its harmonics are also plotted.

shows that (i) harmonics up to $7f_1$, $5f_2$ and $4f_3$ are visible and (ii) almost all combinations $nf_j + f_k$, where n = 2, 3, 4 are observed.

2.5 Local time distribution

On the average, there is a 12 % probability to detect a MSW event within a given hour period. It has been shown that there are only a few events detected between 0300 and 0900 LT. Maxima of occurrence are observed around noon and midnight. For these periods there is a 50 % probability of observing magnetosonic waves. In the afternoon and evening sectors, the probability is of the order of 30 %.

2.6 Dependence on radial distance and geomagnetic latitude

GEOS 1 has explored regions between $L \sim 4$ and $L \sim 8$, in a magnetic latitude range $-15^{\circ} < \lambda_{\rm m} < +30^{\circ}$. Most emissions occur in a restricted range of $\lambda_{\rm m}$, i.e. when the spacecraft is close to the magnetic equator ($\lambda_{\rm m} < 10^{\circ}$). There does not seem to be a specific range of L values (between 4,5 and 7 at least) where these emissions can be observed. These findings are consistent with those of Ref. 3.

3. MSW'S AND PROTON RING DISTRIBUTION

3.1 Experimental results

The wave phenomena described above occurred near the proton gyrofrequency and its harmonics; therefore protons are likely candidates for destabilizing them. The two-

dimensional particle data analyzed in this section were measured on board GEOS by two experiments: (i) S 310 (Kiruna Geophysical Institute), which covers ion energies ranging from 0.3 to 20 keV (Ref. 6) and (ii) S 321 (Max-Planck Institut für Aeronomie), which covers the ion energies ranging from 20 to 3300 keV (Ref. 7). From the differential energy spectra obtained over 45 s or 3 min for S 310 and over 5 min for S 321, the phase space density, f(v) can be determined through the relation:

$$f(v) \propto \frac{J(E, \alpha)}{E}$$
 (cm⁻² s⁻¹ sr⁻¹ keV⁻²)

where $J(E, \alpha)$ is the differential proton flux. The proton data presented here consist of three complementary plots (Figure 3). On the left-hand side, are represented the energy spectra for some characteristic pitch-angles: 90°, 120° and 160°. In the middle panel the pitch angle distributions for various typical energies are plotted. In this study, the selected energies are those close to the peak of the energy spectrum, which provides the free energy source. On the right-hand side isocontours of the phase space density in the $(v_{//}, v_{\perp})$ velocity space are drawn; only a fraction of the $(v_{//}, v_{\perp})$ space is explored during a spin period of GEOS 1. This last plot is of particular interest for studying wave-particle interactions since it shows that $\partial f/\partial v_1 > 0$, while waves are observed corresponding to a peak around 7 keV, as evidenced by the middle panel of this figure. This peak is not only energydependent, but it also depends upon the pitch angle. The largest maximum is obtained for pitch angles close to 90° in a limited energy range. This is confirmed by the right panel where two distinct peaks are clearly visualized: one for $U_1 \sim 1250$ km/s and the second one at $U_1 \sim 1850$ km/s. g to their shape in the v_1 , v_1 plane, these peaks will eferenced to as rings. For this event, the energetic con density, computed by a standard method is $= 1.6 \text{ cm}^{-3}$, whereas the total density is $N_{tot} = 65 \text{ cm}^{-3}$ eading to $\rho = n_r/N_{tot} = 0.02$. At the same time, harmonic emissions are detected in the ULF range. The fundamental f_1 is equal to $1.8 F_H$ + and the first harmonic is clearly seen. The second one is not well defined. The amplitude at f_1 is 10 my. Therefore, ring-like distributions of protons provide the free energy for MSW's growth. However, it should be mentioned that ring-like distribution functions of protons were always found when magnetosonic waves were detected.

3.2 MSW's growth rate calculations

Motivated by these observations, we have computed the growth rate of magnetosonic waves by considering a simple theoretical model that includes a cold plasma plus a ringlike distribution characterized by

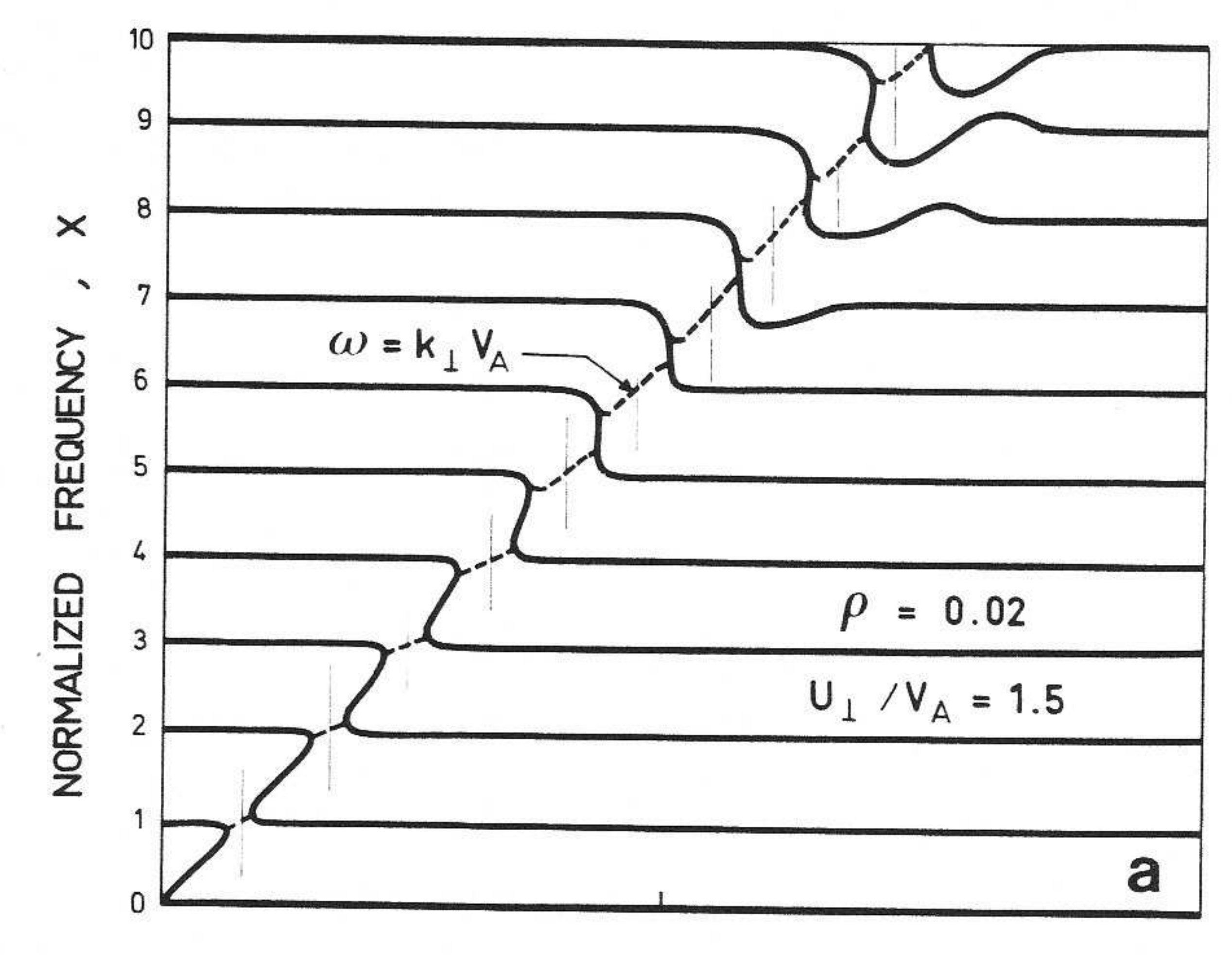
$$f = \frac{n_r}{2\pi V_L} \delta(V_{\parallel}) \delta(V_L - U_L) + \frac{N_c}{2\pi V_L} \delta(V_{\parallel}) \delta(V_L)$$

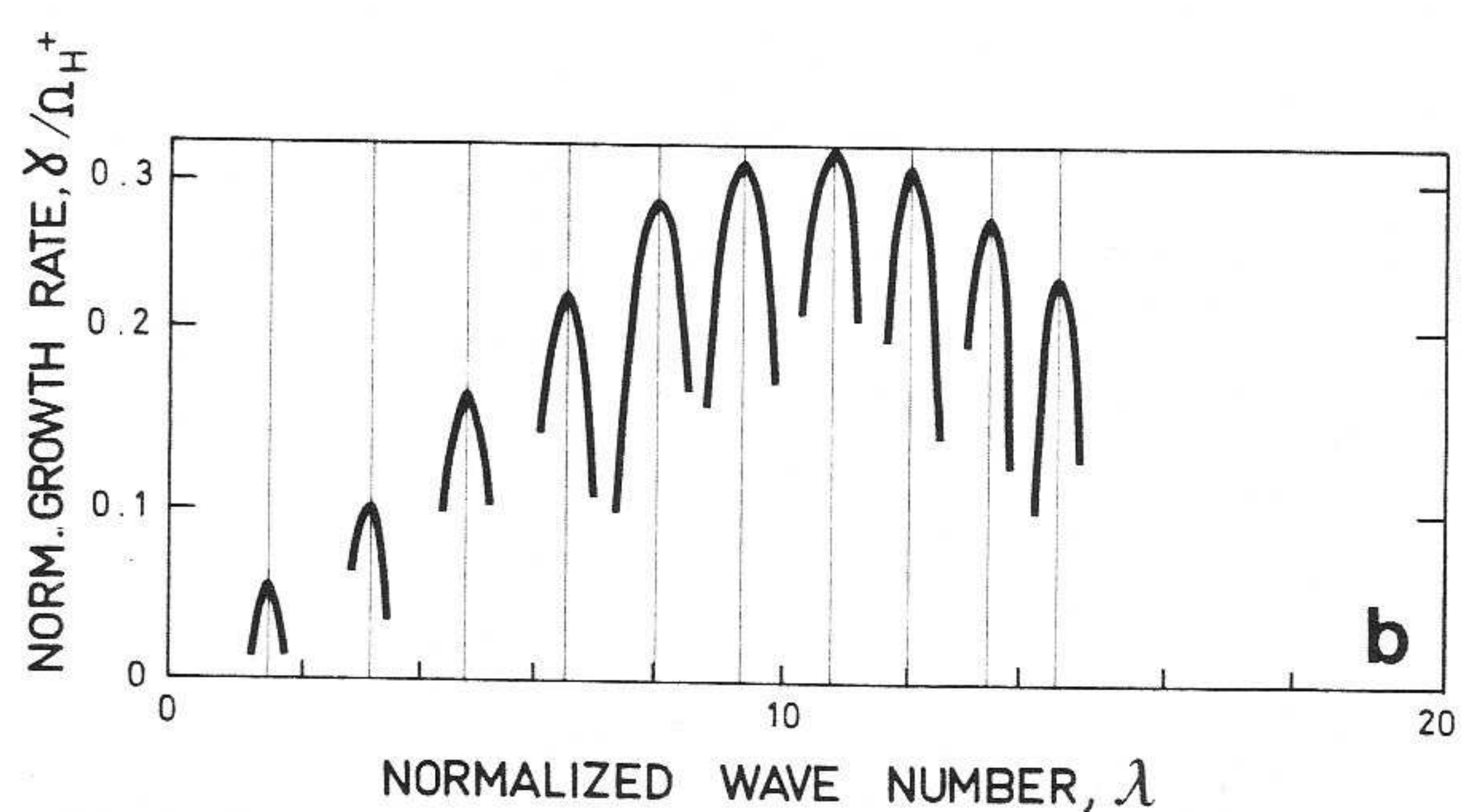
where n and N are the ring and cold plasma densities, respectively, and U₁ is the ring velocity in the perpendicular direction. It is important to emphasize that the instability that is investigated here is basically a hydromagnetic instability, since it still operates when $k_{//} = 0$. Accordingly, the growth rate depends upon the beam density rather than upon the slope $\partial f/\partial v_1$ as it would have had for a kinetic instability. Of course, for a small but finite k_{//} and a smoother distribution of protons, one has to take" care of both effects in order to determine the exact numerical value of the growth rate. The results of these computations performed with parameters fitted with data presented in Figure 3 are presented in Figure 4. For low density rings ($\rho = 0.02$) the computations show that the growth rate γ is only positive when the average velocity of the ring is larger than the Alfven velocity $(U_1/V_{\Delta} > 1)$. It maximizes where the cold plasma dispersion curve ($\omega = k_1 V_A$) intersects the "ringlike" solutions $(\omega = n\Omega_{H}+)$. The growth rate increases with n, which may explain why sometimes only the higher harmonics are observed.

The growth rate calculations carried out here as well as those performed in Ref. 8 lead to the conclusion that wave growth is limited to the near vicinity of the various gyroharmonics (at least for a weak ring). Many observed events do present such a structure. However, as emphasized in part 2, some events have a fundamental frequency that is not close to F_H+, but still exhibits a clear harmonic structure. For instance, one can have $F_1 = 1.5 F_{H^+}$, $F_2 = 3F_{H^+}$, etc. Such a frequency spectrum cannot a priori be described by the present growth rate calculations. One likely possibility is that magnetosonic waves are, in their source region, generated at F_n = nF_H+ by the present mechanism and then, while propagating inward or outward (Ref. 9), penetrate in regions where FH+ is different: accordingly, their normalized frequencies vary, thus explaining why locally F + nFH+. The interesting aspect of this interpretation is that one obtains harmonically-related waves everywhere because they had an harmonic structure in their source region.

4. MSW'S AND DRIFT BOUNDARIES

Drift boundaries delimit regions around the Earth into which particles arriving from outside (e.g. the tail) cannot penetrate under quasi-steady conditions. During disturbed periods these boundaries move inwards and strong outward particle density gradients may build up locally. The

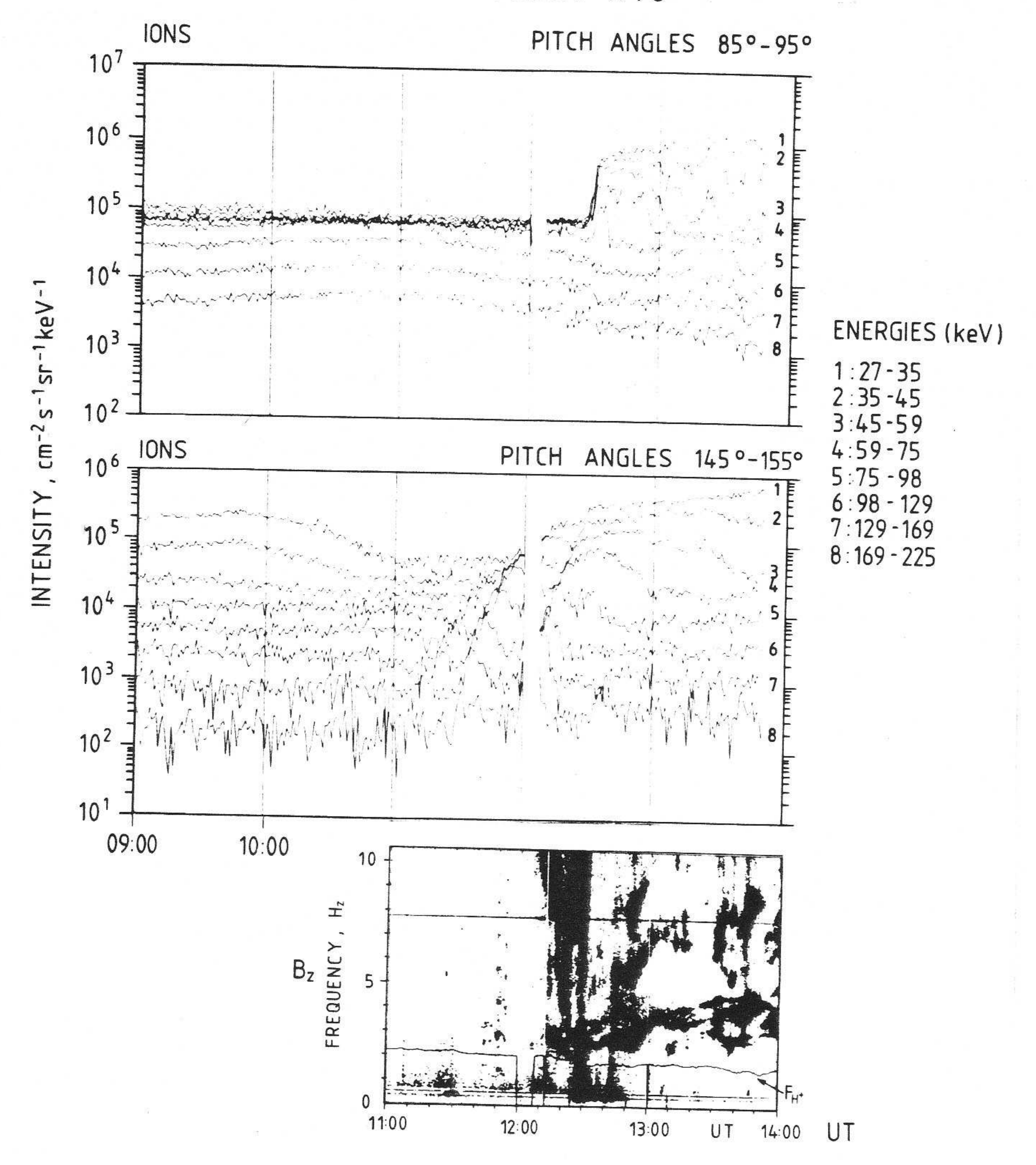




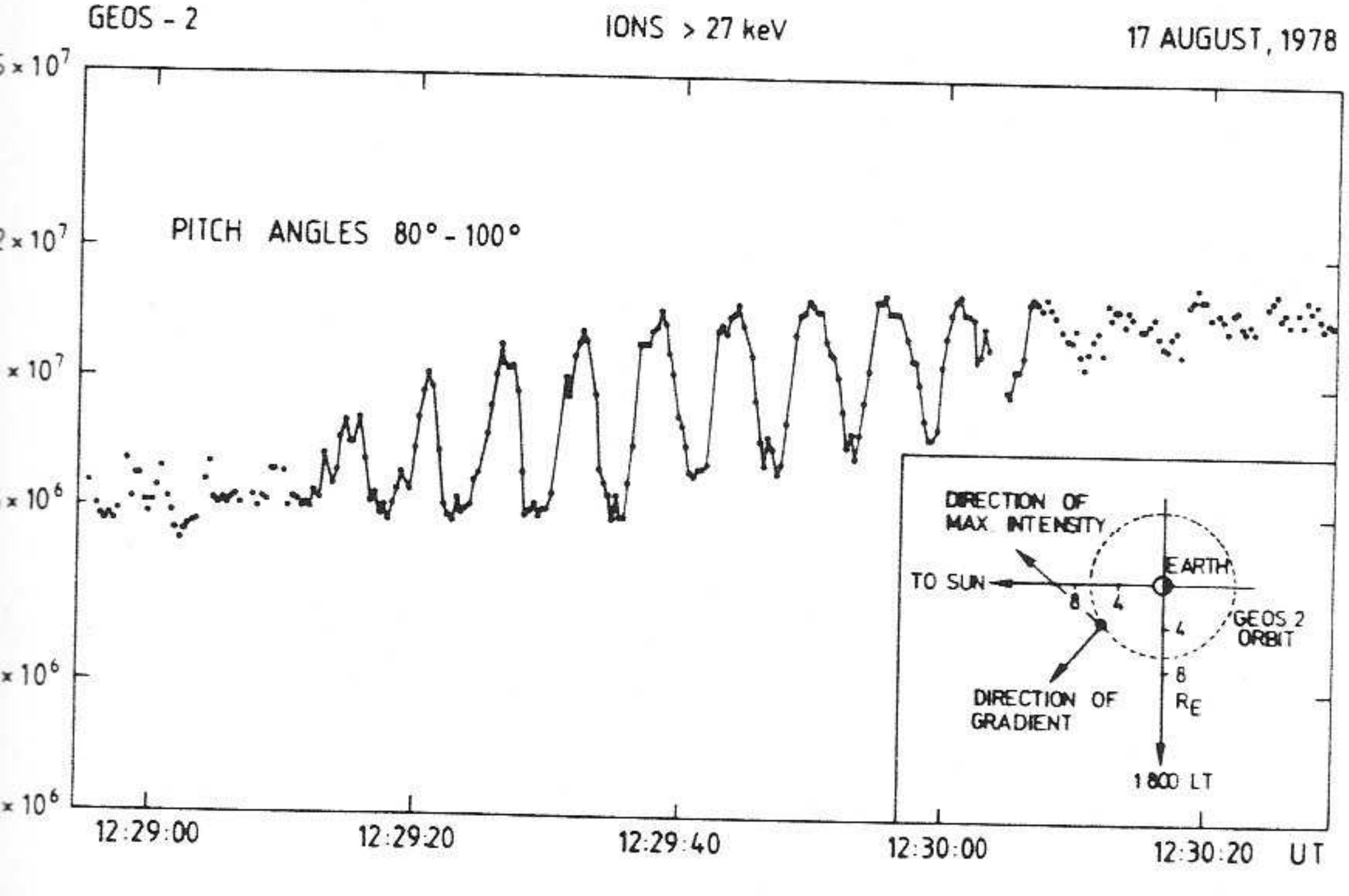
occurrence of such a pressure gradient is illustrated in Figure 5. The top panel shows ion intensities at the pitch angles 90° ± 5° in various energy channels. Before 1229 UT, the ion spectra look fairly flat in the energy range 27-75 keV. At 1229 UT, a sudden intensity increase occurs in each of the five lowest energy channels, and the "normal" monotonically decreasing energy spectrum is thereby restored. The temporal increase shows almost no energy dispersion at pitch angles near 90°.

The middle panel shows ion intensities for the same energy channels but for pitch angle 150° + 5°. In the two lowest energy channels an intensity decrease is observed at 1000 UT and an increase shortly before 1200 UT. Several other intensity increases can be seen in the seventh energy channel (1109 UT, 1126 UT, 1159 UT) that are shifted in time relative to the lower energy channels. The enhanced ion intensities appear first at high energies and then successively at lower energies. The three distinct increases form three profiles that represent the energy-dependent arrivals of drifting ions. Such ions are injected on drift orbits near midnight during substorm activity.

GEOS-2 17 AUGUST 1978



gure 5. Energetic particle data and ULF waves from GEOS 2 for the period 0900-1400 UT on August 17, 1978. From top to bottom are shown differential ion intensities in the energy range 27-225 keV, for pitch angles $90^{\circ} \pm 5^{\circ}$ and a frequency-time spectrogram of the B_Z component, parallel to the satellite spin axis. The angle between the spin axis and the dc magnetic field is about 13°.



ure 6. Spacecraft-spin modulation of ion intensity (E>27 keV) at pitch angles 90° ± 10° for the period 12:29:00 to 12:30:20 UT on August 17, 1978. The direction of the gradient with respect to the GEOS 2 orbit is given in the inset.

During the rapid intensity increase at 1229 UT, large eastwest asymmetries are observed at 90° pitch angle. Figure 6 illustrates this for ions having E > 27 keV at pitch angles 90° + 10°. During each satellite rotation the intensity has one minimum and one maximum. This indicates a spatial gradient in the ion distribution. The gradient points almost radially outward. The maximum of the MSW's intensity is observed when the ion boundary moves across the satellite (fig. 5), thus leading to the conclusion that such a strong gradient provides a free-energy source for destabilizing the (drift) magnetosonic mode. According to Ref. 10, the drift magnetosonic mode is destabilized when $N_{hot}/N_{cold} < \beta/2 (\rho_i/L)^2$. For B = 120 nT, $N_{hot} \simeq 1.3$ cm⁻³ with a peak energy of 20 keV, N_{cold} = 45 cm we find that this instability condition is fulfilled as soon as Li, the scale length of the gradient, is less than two ion Larmor radii. This is what is observed, as evidenced in Figure 6 where flux of energetic ions with 90° pitch angle as a function of the spin phase angle is modulated by 100 %.

5. CONCLUSION

tense magnetosonic waves have been observed to be onfined in the equatorial magnetosphere, with $\delta B/\!\!/B_0$ and hence k1B. Two free energy sources for these waves have been identified: ring-like distribution of protons and strong gradients in the proton pressure. In the latter case, a coupled drift-magnetosonic mode is destabilized. These waves are expected to transfer energy from ten's of keV protons down to low energy protons (<1 keV), which cyclotron damp them.

REFERENCES

- 1. S-300 Experimenters 1979, Measurements of electric and magnetic wave fields and of cold plasma parameters on-board GEOS-1: Preliminary results, Planet. Space Sci., 27, 317-339.
- 2. Perraut S et al 1982, A systematic study of ULF waves above F_H+ from GEOS-1 and -2 measurements and their relationships with proton ring distributions, J. Geophys. Res., 87, 6219-6236.
- 3. Russell C T et al 1970, OGO 3 observations of ELF noise in the magnetosphere, 2, The nature of the equatorial noise, J. Geophys. Res., 75, 755-768.

- 4. Gurnett D A 1976, Plasma wave interactions with energetic ions near the magnetic equator, J. Geophys. Res., 81, 2765-2770.
- 5. Korth A et al 1983, Drift boundaries and ULF wave generation near noon at geostationary orbit, Geophys. Res. Lett., 10, 639-642.
- 6. Borg H L et al 1979, The keV plasma experiment on the GEOS-1 and GEOS-2 satellites, Space Sci. Instrum., 5, 37-49.
- 7. Korth A et al 1978, Observations of substormassociated particle-flux variations at 6 < L < 8 with GEOS-1, Space Sci. Rev., 22, 501-509.
- 8. Gul'elmi A V et al 1975, Excitation of magnetosonic waves with discrete spectrum in the equatorial vicinity of the plasmapause, *Planet. Space Sci.*, 23, 279-286.
- 9. Perraut S 1982, Wave-particle interactions in the ULF range: GEOS-1 and -2 results, Planet. Space Sci., 30, 1219-1227.
- 10. Hasegawa A 1975, Plasma instabilities and nonlinear effects, in *Physics and Chemistry in Space*, vol. 8, Springer, New York.